The 11th Canadian Conference on Earthquake Engineering
Canadian Association for Earthquake Engineering

DIMENSIONAL ANALYSIS OF SLIDING CONTENTS IN SEISMICALLY ISOLATED BUILDINGS UNDER PULSE-TYPE EXCITATION

Farzad NIKFAR
PhD Candidate, McMaster University, Canada
nikfarf@mcmaster.ca

Dimitrios KONSTANTINIDIS
Assistant Professor, McMaster University, Canada
konstant@mcmaster.ca

ABSTRACT: Sliding of building contents, such as equipment, is of primary concern during an earthquake because not only can it contribute to substantial losses due to nonstructural damage, but also pose a serious safety risk to building occupants. In this study, dimensional analysis is performed to explore the existence of physical similarities in the sliding response of equipment and contents in base-isolated buildings. Buckingham's π-theorem is used to introduce dimensionless π terms and the corresponding governing dimensionless equation. In this investigation, pulse-like ground motions are approximated by analytical pulses. The contents are idealized as freestanding rigid bodies, free to slide but not rock. The mechanical behaviour of the contact surface between the contents and the building floors is described by a Stribeck friction model taking into account the transition from static to kinetic friction. The base-isolated building is treated as a rigid mass supported on viscously damped linear isolators. The effect of various parameters, including isolation nominal period and damping, static friction and its transition to kinetic friction, and interaction between the sliding object and the seismically isolated building are investigated. The study shows that the peak sliding response of rigid objects exhibits complete similarity in the ratio of kinetic to static friction coefficient. Hence, assuming a simple Coulomb friction model with a single friction coefficient parameter is adequate when peak sliding displacement is the main concern; although presence of static friction does change the response history and permanent displacement. Moreover, it is observed that as the damping increases, the response exhibits complete similarity in the ratio of isolation frequency to pulse frequency. The study concludes that certain combinations of the isolation system design parameters can result in amplification in the peak sliding response of contents, compared to the fixed-base building.

1. Introduction

The resilience of a wide range of buildings housing important nonstructural components and systems (NCS), also referred to as Operational and Functional Components (OFC), is highly correlated to the seismic performance of these NCS. For critical facilities, such as hospitals, emergency operations centers, and power plants, continued functionality during and after a seismic event is of utmost importance. While the most rigorous performance level, i.e., *immediate occupancy*, is usually targeted in the design process of such critical buildings, this does not necessarily guarantee acceptable performance of the NCS. From the economic point of view, neglecting NCS is imprudent. Their value in a typical commercial building dwarfs the cost of the structure itself, often accounting for 80 to 90% of the total value of a building (Taghavi and Miranda, 2003). In view of this and the fact that nonstructural damage typically occurs at lower levels of shaking intensity than structural damage, it is expected that a significant portion of economic losses resulting from a major seismic event will be attributed to nonstructural damage (Comerio, 2005).

A typical building houses a very wide collection of NCS. In this study, we focus on building Equipment

and Contents (EC) for which sliding is the only mode of response. Sliding is very common for freestanding (i.e., unrestrained) EC, particularly those that are stocky and have a relatively low friction coefficient. Although seismic restraints are typically recommended to prevent sliding of EC, such restraints can be costly. For example, in UC Berkeley buildings where the dominant use is laboratories, the cost of seismic restraining of the EC could range from US$8 to $12 million (Comerio and Stallmeyer, 2002). Besides cost, there are also practical limitations associated with restraining EC. Some EC items need to remain mobile (Dar et al., 2015). Another problem associated with restrained EC is that they can exhibit significantly larger accelerations compared to freestanding EC (Konstantinidis and Makris, 2005).

The hazard associated with freestanding sliding EC can stem from one or combination of: (a) excessive sliding displacement, regardless of velocity and acceleration, that can result in the EC falling off the edge of its support surface, or, in the case of large heavy EC, blocking an evacuation path or doorway; (b) impact due to large sliding displacement and velocity that can put the safety of the people working in the vicinity of the EC or the functionality of the EC at risk; and (c) large accelerations, particularly in the high frequency range, that can cause resonance and damage to the electronic parts of EC. Therefore, desirable characteristics of earthquake protection systems for EC include the ability to decrease floor acceleration, sliding velocity, and sliding displacement together with shifting the floor vibration frequency to frequencies lower than the content resonance frequency. Seismic isolation appears to be an ideal solution for protecting a building's EC since it aims to control all of the aforementioned parameters. While this claim has been made three decades ago (Kelly and Tsai, 1985), the supporting research for unattached EC is fairly new. Nikfar and Konstantinidis (2013) studied the performance of sliding EC in isolated buildings under broad-band and pulse-like ground motions. Sliding fragility curves for broad-band ground motions are presented in (Konstantinidis and Nikfar, 2015). As shown in the parametric studies presented in (Nikfar and Konstantinidis, 2013), the dynamic response of sliding EC under pulse-like ground motions is considerably different than broad-band ground motions.

In this study, dimensional analysis is performed to explore the existence of physical similarities in the sliding response of EC in base-isolated buildings under pulse type excitations. Buckingham's π-theorem is used to introduce dimensionless π-terms and the corresponding governing dimensionless equation. The Stribeck friction model that takes into account the velocity dependence of friction is assumed to describe the contact interface between the EC and their base. The effect of various parameters on the sliding response of EC is investigated, including the ratio of the isolation to pulse period, isolation damping, ratio of static to kinetic friction, parameters associated with velocity-dependent friction, and interaction between sliding contents and isolated building.

2. Model of Structure and EC

A seismically isolated building and its sliding EC can be mathematically described by the three degree-of-freedom (DOF) dynamic system shown in Figure 1-a. In this model, u_s is the displacement of the EC relative to the floor (i.e., the sliding displacement), u_1 represents horizontal displacement (deformation) of the isolation layer, and u_2 horizontal displacement of the story relative to the ground. The horizontal displacement of the ground is u_g. For simplicity, the vertical component of ground motion is neglected in this study. m_{st} represents the mass of the superstructure. The base isolation system consists of a base floor of mass m_b on a viscously damped linear elastic isolation system, i.e., a viscoelastic system. This model was used early on to introduce the linear theory of seismic isolation (Kelly, 1997) and continues to be used widely, primarily due to its simplicity. The numerical efficiency of this linear model lends itself to large parametric investigations (Yang et al., 2010). The model consists of a linear spring of stiffness k_b in parallel with a linear viscous damper of damping coefficient c_b. Using this model, the nominal period T_b and damping ratio ξ_b of the isolated system are given by (Kelly, 1997)

$$T_b = 2\pi\sqrt{\frac{m_{st}+m_b}{k_b}} \quad , \quad \xi_b = \frac{c_b}{2\sqrt{k_b(m_{st}+m_b)}} \tag{0}$$

The definition for the nominal fundamental period and damping ratio of the isolated structure, given by Equation 0, are based on the premise that in a seismically isolated building, the superstructure moves as a nearly rigid body on a very flexible base. In reality, the fundamental period of the system is slightly larger than the nominal period. If assuming a base isolated building like the one shown in Figure 1-a, it is reasonable to treat the superstructure as a rigid structure supported on a very flexible base, thus reducing

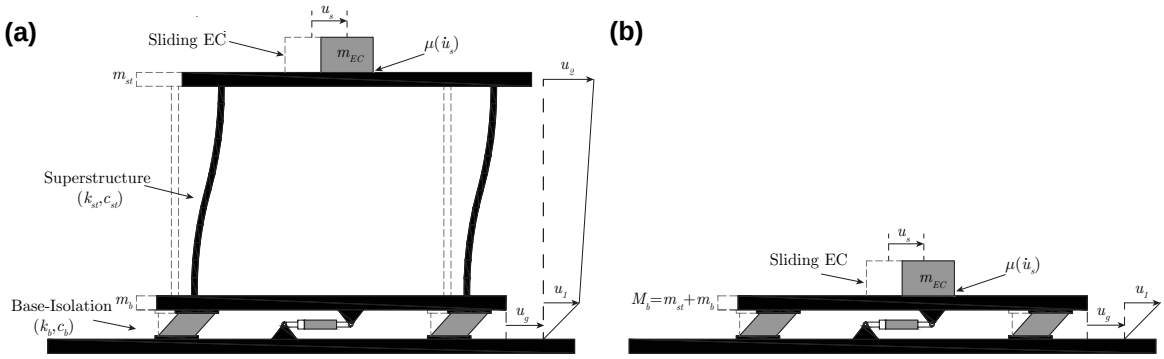

Figure 1 – (a) Linear seismic isolation model. (b) SDOF representation of the seismic isolation model (assuming a very stiff superstructure relative to the isolation layer).

the base isolated structure to a single degree of freedom system (Konstantinidis and Nikfar, 2015) as shown in Figure 1-b. Treating the base isolated building as a SDOF system reduces the number of variables involved in the dimensional analysis by two and simplifies the interpretations of the effect of each parameter on the response of the system.

A rigid block of mass m_{EC} on an isolated base is considered to represent the EC, as Figure 1-b. The contact friction is defined using a *Stribeck* friction model that takes into account the rate dependence of friction as illustrated in Figure 2. A Stribeck friction model that can take into account both static, μ_s, and kinetic, μ_k, friction coefficients and the transition between the two expressed by a hyperbolic secant function, as suggested in (Xia, 2003), as well as viscosity at the contact, can be expressed by

$$\mu(\dot{u}_s) = \mu_s \operatorname{sech}(\dot{u}_s\beta) + \mu_k\left(1-\operatorname{sech}(\dot{u}_s\beta)\right) + \gamma_n\left|\dot{u}_s\right|^n \quad \textbf{(}n=1\textbf{, in this study)} \tag{1}$$

In this equation, $\dot{u}_s$ represents sliding velocity; constant β defines the transition sharpness from static to kinetic friction; and γ represents viscous characteristics of the contact. The first two terms of Equation 1 account for the smooth transition from static to kinetic friction. The larger β, the sharper the transition, as shown in Figure 2. Kinetic friction itself is defined as a velocity-dependent parameter. The last term of Equation 1, $\gamma_n\left|\dot{u}_s\right|^n$, captures any nonlinear viscous velocity dependence of friction, known as *viscous contact*. This definition is well explained in mechanical engineering literature, specifically for friction between lubricated surfaces. However, velocity dependence of kinetic friction is not limited to lubricated surfaces and has been observed in dry friction experiments as well. Depending on the surface characteristics, the actual behaviour may be approximated by a linear or nonlinear function, $\gamma_n\dot{u}_s^n$. For simplicity, n is assumed to be equal to unity in Equation 1, representing linear viscous damping for the contact. The friction force for the sliding block under horizontal excitation is defined by

$$F_f = \mu(\dot{u}_s) m_{EC} g \operatorname{sgn}(\dot{u}_s) \tag{1}$$

in which sgn(·) represents *signum* function. The dynamic equation of motion of the system including the sliding EC, superstructure, and isolation system is constructed in state- space form and solved using

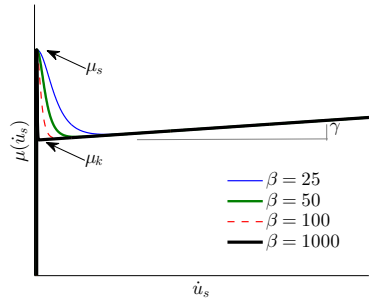

Figure 2 – Stribeck friction model

MATLAB ODE solver. A bilinear model with very large initial stiffness is assumed to approximate the signum function of Equation 1. The procedure to solve such dynamic systems with path-dependent nonlinearities, i.e., bilinear hysteresis restoring forces, is explained in detail by the authors in (Nikfar and Konstantinidis, 2014).

3. Dimensional Analysis

3.1. Introduction

Dimensional analysis is employed to reveal the underlying physics in the sliding of EC in seismically isolated buildings as well as to demonstrate the complete- and self-similarities in the response of the system. Analytical pulses are used since dimensional analysis requires a time scale and a length scale of the ground excitation. To demonstrate the concept of the length scale of a pulse excitation, assume a rigid sliding block of mass m on the ground that is subjected to a rectangular horizontal acceleration pulse as shown in Figure 3-a. Provided that a Coulomb friction force resists the sliding of this rigid block, the early solution for rigid-plastic system presented by (Newmark, 1965) describes the maximum sliding displacement of the block (Figure 3-b) as

$$u_{max} = \frac{a_p T_p^2}{2}\left(\frac{a_p}{\mu g} - 1\right) \quad , \quad (a_p > \mu g) \tag{2}$$

Equation 2 shows that $u_{\max}$ is proportional to the so-called *characteristic length scale* of the excitation, $L_p = a_p T_p^2$, and the *intensity* of the pulse which is presented by the terms within the parenthesis in Eq. 2. The characteristic length scale represents the persistence of the excitation in displacing the object (Vassiliou and Makris, 2011). As it is shown in Figure 3-c, after expiration of this pulse, the ground moves with constant velocity, eventually resulting in infinite ground displacement. However, such a pulse is not physically realizable. In order for a pulse to generate finite displacement, the area under the acceleration time-history must be zero (i.e., zero mean acceleration); in other words, the final velocity must be zero. In addition to that, the energy released by earthquake shaking is always finite.

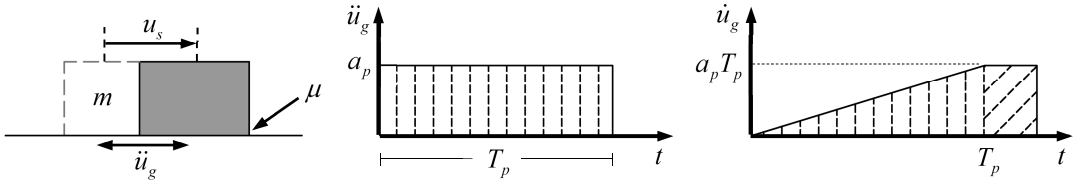

(a) **(b)** **(c)**

Figure 3 – (a) Rigid sliding block subjected to a horizontal ground excitation. (b) Rectangular ground acceleration pulse with amplitude a_p and duration T_p. (c) Ground velocity.

This means that the area under the square of the pulse must be finite. Because of the aforementioned conditions, wavelets are commonly utilized for the characterization of different pulses in actual ground motions. A wavelet is a waveform (signal), $\varphi(t)$, in time domain that satisfies the finite energy and zero mean conditions,

$$E = \int_{-\infty}^{\infty} \left|\varphi(t)\right|^2 dt < \infty \tag{3}$$

$$\int_{-\infty}^{\infty} \varphi(t) dt = 0 \tag{3}$$

In Figure 4, the long-period pulse of the RSS228 motion recorded during 1994 Northridge earthquake is approximated using the symmetric Ricker wavelet with effective period of $T_p = 1\,\text{s}$. The symmetric Ricker wavelet is basically the second derivative of the Gaussian distribution, $e^{-t^2/2_p}$, described by (Vassiliou and Makris, 2012)

$$\varphi(t) = a_p\left(1 - \frac{2\pi^2 t^2}{T_p^2}\right) e^{-\frac{1}{2}\frac{2\pi^2 t^2}{T_p^2}} \tag{3}$$

where $T_p = 2\pi/\omega_p$ is the period corresponding to the peak Fourier spectrum of the wavelet. Analytical pulse excitations such as Ricker wavelet, if being consistent to the coherent pulse, can approximately simulate the kinematics of pulse-like ground motions that are known as one of the most destructive class of ground motions to most civil structures (Bertero et al., 1978; Somerville and Graves, 1993; Hall et al., 1995). The capability of the closed-form analytical pulses to simulate real ground motions for studying structural response has been investigated at various scales (Veletsos et al., 1965; Hall et al., 1995; Makris, 1997; Mavroeidis and Papageorgiou, 2003; Makris and Black, 2004) among others. Various analytical two- and four- parameter pulses have been proposed. The Ricker wavelet is used in the demonstrations of the dimensionless master curves in this study.

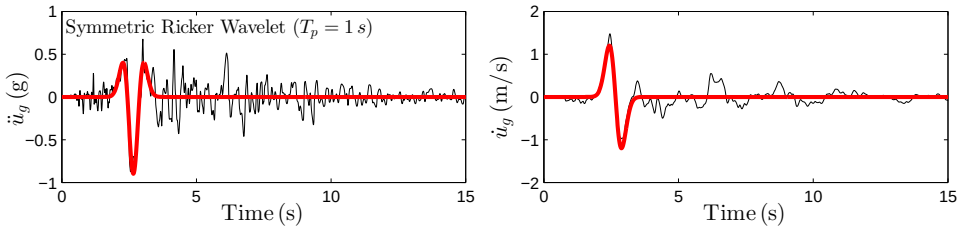

Figure 4 – (a) Ground acceleration and velocity time histories of the 1994 Northridge earthquake recorded at Rinaldi Receiving Station together with the symmetric Ricker wavelet with effective period of 1 s matched to the long-period pulse.

3.2. Dimensional analysis of the sliding objects on viscoelastic base

Referring to the model presented by Figure 1-b and based on Equation 1, the maximum sliding displacement of EC on a viscoelastic base, as a dependent variable, under an excitation with coherent pulse acceleration amplitude a_p and period T_p is expected to be a function of ten independent variables (for each pulse type)

$$u_{\max} = f(a_p, T_p, M_b, T_b, \xi_b, m_{EC}, \mu_s, \mu_k, \beta, \gamma, \text{shape of pulse}) \tag{4}$$

where $T_b = 2\pi\sqrt{M_b/k_b}$. In Equation 4, the eleven variables, having dimensions $u_{\max} \doteq [L]$, $a_p \doteq [L][T]^{-2}$, $T_p \doteq [T]$, $T_b \doteq [T]$, $M_b \doteq [M]$, $m_{EC} \doteq [M]$, $\xi_b \doteq [\cdot]$, $\mu_s \doteq [\cdot]$, $\mu_k \doteq [\cdot]$, $\beta \doteq [L]^{-1}[T]$ and $\gamma \doteq [L]^{-1}[T]$, involve all three reference dimensions, that of mass $[M]$, length $[L]$ and time $[T]$. Based on Buckingham's π-theorem the number of independent dimensionless π-terms is equal to the number of variables in Equation 4 (eleven variables) minus the number of reference dimensions (three) leading to eight dimensionless π-products. Repeated variables should contain the parameters representing the pulse characteristics, i.e., a_p and T_p, together with M_b. Consequently, the dimensionless π-products considered are

$$\Pi_1 = \frac{u_{\max}}{a_p T_p^2},\ \Pi_2 = \frac{\mu_k g}{a_p},\ \Pi_3 = \frac{T_b}{T_P},\ \Pi_4 = \xi_b,\ \Pi_5 = \frac{\mu_k}{\mu_s},\ \Pi_6 = \beta a_p T_p,\ \Pi_7 = \gamma a_p T_p,\ \Pi_8 = \frac{m_{EC}}{M_b} \tag{5}$$

Therefore, the resultant dimensionless equation takes the form

$$\Pi_1 = \Phi(\Pi_2, \Pi_3, \Pi_4, \Pi_5, \Pi_6, \Pi_7, \Pi_8, \text{shape of pulse}) \tag{6}$$

where Φ is the function that can be obtained either analytically, if a closed-form solution exists, or numerically, for each pulse type. Reduction in the number of variables by three results in self-similar solutions for Equation 6 with respect to the repeated variables chosen. In other words, the dimensionless solutions will be the same for all the values of a_p, T_p and M_b. By expressing the behaviour in terms of dimensionless products, the effects of different parameters on the response can be examined.

3.2.1. Effect of the isolation period ($\Pi_3 = T_b/T_P$)

Π_3 is the measure of the relative stiffness of the isolation system. Small values of Π_3 (e.g., $\Pi_3 < 0.01$) represents no isolation, while large values represent a large degree of isolation. Figure 5 (left) plots the so-called dimensionless master curves for various Π_3 values, while other π-terms are fixed. These curves

are presented for 10% isolation damping ($\Pi_4 = \xi_b = 0.1$). The term master curve refers to the self-similar curves with respect to the repeating variables that in this study are a_p, T_p and M_b. The presented curves are the same for all possible combinations of values of these three parameters. In this context, the vertical axis, $\Pi_1 = u_{\max}/a_p T_p^2$, represents the dimensionless displacement, and the horizontal axis, $\Pi_2 = \mu_k g/a_p$, represents the dimensionless frictional resistance. Each of $\Pi_5 = \mu_k/\mu_s = 1$ or $\Pi_6 = 0.0$ in these plots eliminates the static phase of friction and therefore denotes the case with Coulomb friction model. Note that 1000 s/m is the maximum value for β used in this study, representing a sudden drop from static to kinetic friction coefficient. Dynamic interaction between the sliding object and the isolation system is avoided by considering a mass ratio as small as $\Pi_8 = m_{EC}/M_b = 10^{-5}$. Considering the $\Pi_3 = 0.01$ curve to represent a very stiff isolation system, or effectively a fixed-base system, we notice that seismic isolation does not necessarily decrease the maximum sliding demand for all the values of isolation period and friction. The amplification happens specifically for low friction coefficient values, while generally the demand drops compared to the stiff system by increasing the friction coefficient. The highest amplification is associated with the resonance condition, where the isolation period is very close to the pulse period. Moreover, the effect of the isolation damping in displacement reduction is evident in the resonance condition ($\Pi_3 = 1.0$), while it has marginal effect for non-resonance cases.

3.2.2. Effect of the isolation damping ($\Pi_4 = \xi_b$)

Figure 5 (right) demonstrates the effect of isolation damping under the resonance condition, $\Pi_3 = 1.0$, on the sliding of EC. Providing a minimum amount of damping, i.e., 10%, considerably reduces the sliding response. However, the efficiency drops rapidly for damping values grater that 15%.

3.2.3. Effect of the ratio of kinetic to static friction coefficient ($\Pi_5 = \mu_k/\mu_s$)

Π_5 represents the ratio of kinetic to static friction coefficient. $\Pi_5 = 1$ indicates Coulomb friction model (where $\mu_s = \mu_k$), while values lower than unity describe Stribeck friction that itself subsumes the Static+Coulomb friction model when $\Pi_6 \to \infty$ (e.g., $\beta \to \infty$), leading to a sudden drop from static to kinetic friction. The practical range of Π_5 changes based on the properties of the problem being investigated. For instance, experimental tests on light science laboratory equipment items (Chaudhuri and Hutchinson, 2005) showed Π_5 to range between 0.73 and 1.0, while tests on heavy laboratory equipment (Konstantinidis and Makris, 2005; Konstantinidis and Makris, 2009) measured Π_5 to range between 0.72 and 0.77. Based on those observations, a lower bound value of $\Pi_5 = 0.5$ is assumed in this study. The dimensionless curves (master curves) demonstrating the effect of Π_5 on the maximum sliding response are presented in Figure 6 for three different isolation-to-pulse period ratios and 10% isolation damping. The dimensionless curves are obtained for $\beta = 1000$ s/m (e.g., $\Pi_4 = 1000 a_p T_p$). Presence of static friction reduces the maximum sliding response for large values of Π_2, while it results in amplification for low values of Π_2. Therefore, neglecting the static phase of friction, as being done when using the Coulomb friction model, is unconservative when estimating the maximum sliding displacement of contents with low friction.

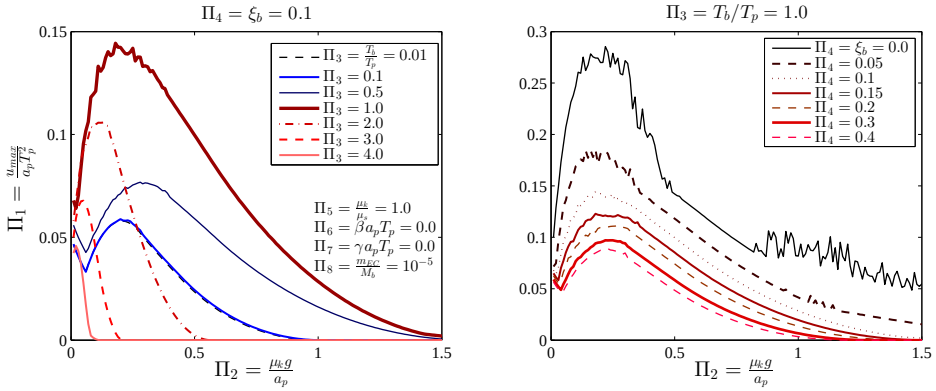

Figure 5 – Dimensionless solutions to demonstrate the effect of isolation period ratio $\Pi_3 = T_b/T_P$ (left) and isolation damping $\Pi_4 = \xi_b$ (right).

This finding may be one of the reasons explaining why the Coulomb friction model underestimated the actual sliding displacements of the heavy laboratory equipment in experimental tests (Konstantinidis and Makris, 2005; Konstantinidis and Makris, 2009). Observations like this highlight the profound advantage of dimensional analysis, which can be used to study the behaviour of a complicated problem by condensing a number of curves in only one master curve. Otherwise, a comprehensive parametric study would be necessary to arrive at such a conclusion. The amplification under the symmetric Ricker wavelet excitation is attributed to the resistance of the system with high static friction to the first pulse of the Ricker wavelet which results in one directional sliding under the major pulse of the excitation. In other words, for $\Pi_5 = 1$, sliding of the EC under the first minor pulse of the Ricker excitation in the negative direction cancels out a portion of the sliding in positive direction under the major pulse of the Ricker wavelet, resulting in smaller maximum sliding displacement. Therefore, even though presence of a static friction increases the overall strength (resistance) of the system, it may result in amplification effects due to the presence of preceding or succeeding pulses close to the major pulse in real earthquake excitations. Such sensitivity in sliding response calls for more accurate estimations of the kinematics of pulse-like ground motions, when analytical pulses are to be used. Moreover, as can be seen in Figure 6, there is a similarity in maximum sliding response in the range of sliding equipment tested previously ($0.7 \le \Pi_5 \le 1.0$). Consequently, one may assume that Π_1 is almost independent of Π_5 (and consequently Π_6) in that range and simplify the dimensionless sliding equation to:

$$\begin{cases} \Pi_1 \approx f(\Pi_2, \Pi_3, \Pi_4, \Pi_7, \Pi_8) & \text{for} \quad 0.7 \le \Pi_5 \le 1.0 \\ \Pi_1 \approx f(\Pi_2, \Pi_3, \Pi_4, \Pi_5, \Pi_6, \Pi_7, \Pi_8) & \text{for} \quad \Pi_5 \le 0.7 \end{cases} \tag{7}$$

3.2.4. Effect of transition sharpness ($\Pi_6 = \beta a_p T_p$) and viscous contact parameter ($\Pi_7 = \gamma a_p T_p$)

The effect of the transition parameter Π_6 on the sliding response is examined by computing the dimensionless curves for $10 a_p T_p \le \Pi_6 \le 1000 a_p T_p$. The master curves are presented in Figure 7 (left). The curves are close to each other in the range of interest for this parameter. Consequently, since changing Π_6 by two orders of magnitude results in relatively comparable master curves, it can be said that the dimensionless sliding response, Π_1, exhibits *complete similarity* in Π_6. Hence, the simplified dimensionless maximum sliding equation described by Equation 7 becomes

$$\begin{cases} \Pi_1 \approx f(\Pi_2, \Pi_3, \Pi_4, \Pi_7, \Pi_8) & \text{for} \quad 0.7 \le \Pi_5 \le 1.0 \\ \Pi_1 \approx f(\Pi_2, \Pi_3, \Pi_4, \Pi_5, \Pi_7, \Pi_8) & \text{for} \quad \Pi_5 \le 0.7 \end{cases} \tag{8}$$

If assuming no viscous damping at the contact, i.e. $\Pi_7 \to 0$, and neglecting the dynamic interaction between the content and isolation system by assuming a very small mass for the EC, i.e. $\Pi_8 \to 0$, the dimensionless sliding displacement, Π_1, for a massless rigid sliding block is approximately a function of only Π_2 in the range observed for sliding EC, i.e., $0.7 \le \Pi_3 \le 1.0$. Here, the dimensional analysis proved the dominant role of kinetic friction on the maximum sliding response in its general form, which has been observed in previous investigations (Newmark, 1965; Konstantinidis and Makris, 2005; Chaudhuri and Hutchinson, 2005; Hutchinson and Chaudhuri, 2006; Konstantinidis and Makris, 2009; Konstantinidis and Makris, 2010). Only a handful of experiments are available for evaluating the velocity dependence of

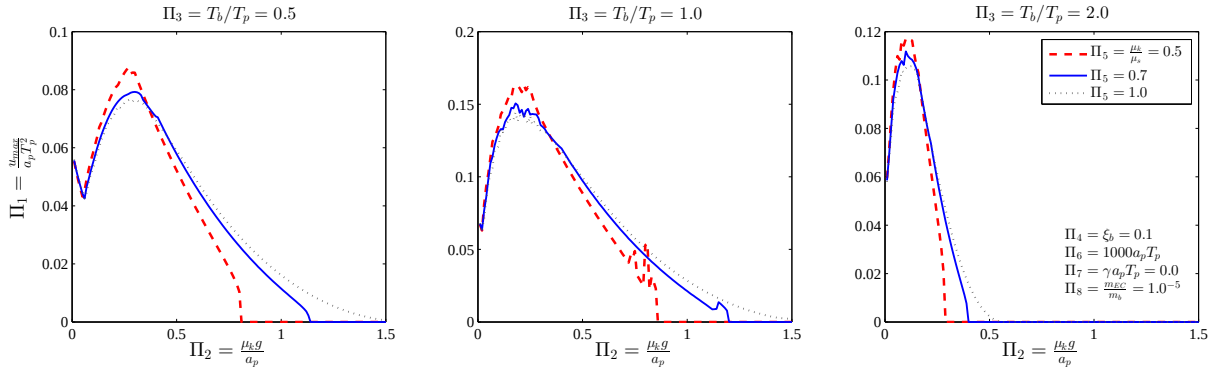

Figure 6 – Effect of kinetic-to-static friction coefficient ratio $\Pi_5 = \mu_k / \mu_s$.

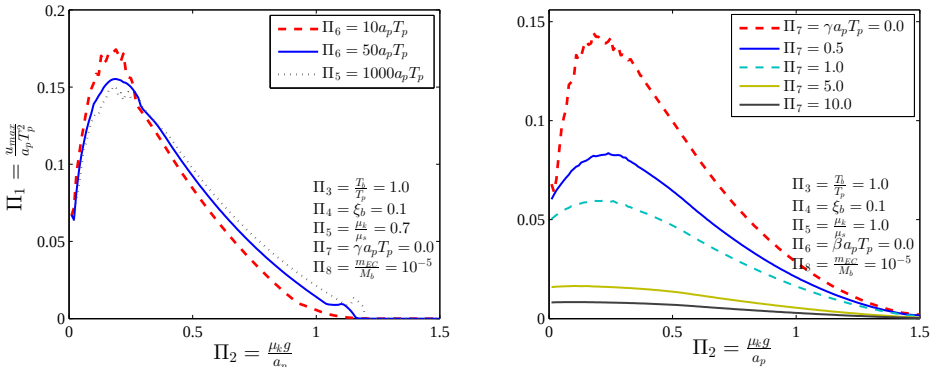

Figure 7 – Left: Effect of the transition between static and kinetic friction, $\Pi_6 = \beta a_p T_p$. Right: Effect of viscous property of the contact, $\Pi_7 = \gamma a_p T_p$.

friction in earthquake engineering. One such study (Konstantinidis et al., 2008) included cyclic testing of sliding bridge bearings, which on average exhibited a maximum γ value of about 0.05. In the dimensional analysis of the current study, the upper bound for Π_7 is determined by assuming $\gamma_{\max} = 0.1\text{s/m}$, $a_{p(\max)} = 2g$, and $T_{p(\max)} = 5\,\text{s}$, resulting in $\Pi_{5(\mathbf{max})} \approx 10$. Figure 7 (right) illustrates how Π_7 affects the sliding response of EC; the higher the contact damping, the lower the sliding response.

3.2.5. Effect of the dynamic interaction between the structure and the EC ($\Pi_8 = m_{EC}/M_b$)

Depending on their friction coefficient and mass, building EC may influence the dynamic response of the building. Heavy EC with high friction coefficient move rigidly with their base, leading to a longer isolation period. EC with low friction coefficient, which are more prone to sliding, may increase the damping of the system by dissipating energy through friction.

Figure 8 shows the effect of the mass ratio on the maximum sliding displacement for isolation periods lower, equal, and larger than the pulse period. For the case where $\Pi_3 = T_b/T_P = 0.1$ (left plot) and the mass of the EC is equal to the isolation mass, the dimensionless sliding displacement parameter, Π_1, decreases for low Π_2, due to the added energy dissipation through friction, and increases for large Π_2. Figure 8 shows that the maximum sliding displacement is not affected by the mass of the EC, even up to a mass ratio of 10%. Hence, the practicing engineer concerned with the maximum sliding of contents may neglect the dynamic interactions if the mass of the sliding contents is less than 10% of the isolation mass.

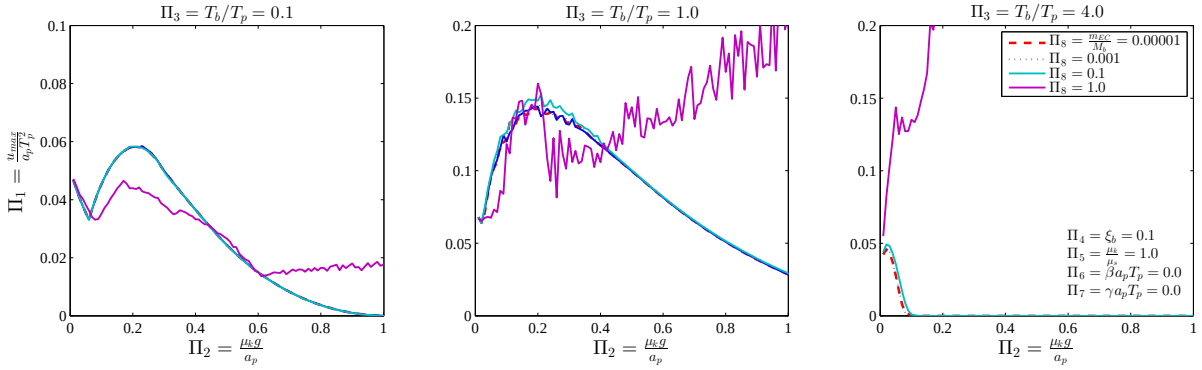

Figure 8 – Effect of the mass ratio $\Pi_8 = m_{EC}/M_b$ on the maximum sliding response.

4. Conclusions

This study presents the results of a comprehensive parametric investigation on the sliding response of equipment and contents (EC) in seismically isolated buildings subjected to pulse excitations through the use of dimensional analysis. The main findings of this research can be summarized as follows:

- Under pulse excitations, amplification occurs in the peak sliding displacement of EC with increasing isolation-to-pulse period ratio, $\Pi_3 = T_b / T_P$, specifically for low $\Pi_2 = \mu_k g / a_p$ (i.e., low friction coefficient values or large acceleration pulse amplitudes). The highest amplification is associated with the resonance condition, where isolation period is very close to the pulse period. For $\Pi_3 > 1$, the dimensionless sliding displacement parameter decreases with increasing $\Pi_3 = T_b / T_P$, demonstrating the decoupling effect associated with isolation.
- Even a relatively small amount of isolation damping, say 10%, is very effective in reducing the sliding displacements under the resonance condition ($\Pi_3 = 1.0$), while damping has marginal effect for non-resonance cases.
- Presence of static friction reduces the maximum sliding response for large $\Pi_2 = \mu_k g / a_p$, while it results in some amplification in the response for low $\Pi_2 = \mu_k g / a_p$. Therefore, neglecting the static phase of friction is not always conservative when estimating the maximum sliding displacement of EC with low friction. However, in the range of static-to-kinetic friction ratio of sliding equipment tested previously ($0.7 \le \Pi_5 \le 1.0$),the maximum sliding response exhibits similarity. Master curves also show that the dimensionless displacement exhibits *complete similarity* in the transition parameter β.
- The dynamic interaction of EC and the isolated base slab is negligible even up to $\Pi_8 = m_{EC} / M_b = 0.1$. Hence, the practicing engineer concerned with the peak sliding of EC may neglect this dynamic interaction if the sliding contents constitute less than 10% of the isolation mass.

5. References

BERTERO, V.V., MAHIN, S.A. and HERRERA, R.A., "Aseismic design implications of near-fault San Fernando earthquake records", Earthquake Engineering and Structural Dynamics, Vol. 6, No. 1, 1978, pp.31–42.

CHAUDHURI, S.R., HUTCHINSON, T.C., "Characterizing frictional behavior for use in predicting the seismic response of unattached equipment", Soil Dynamics and Earthquake Engineering, Vol. 25, No. 7–10, 2005, pp.591–604.

COMERIO, M.C, "PEER testbed study on a laboratory building: exercising seismic performance assessment". Pacific Earthquake Engineering Research Center (PEER) University of California, Berkeley, Report No. 2005/12, 2005.

COMERIO, M.C., STALLMEYER, J.C., "Nonstructural loss estimation:the UC Berkeley case study", Pacific Earthquake Engineering Research Center (PEER) University of California, Berkeley, Report No. 2002/01, 2002.

DAR, A., KONSTANTINIDIS, D., El-DAKHAKHNI, W., “Evaluation of ASCE 43-05 seismic design criteria for rocking objects in nuclear facilities”, Journal of Structural Engineering (under review), 2015.

HALL, J.F., HEATON, T.H., HAILLING, M.W., WALD, D.J., "Nearsource ground motion and its effects on flexible buildings", Earthquake Spectra, Vol. 11, No. 4, 1995, pp.569–605.

HUTCHINSON, T.C., CHAUDHURI, S.R., "Bench-shelf system dynamic characteristics and their effects on equipment and contents", Earthquake Engineering and Structural Dynamics, Vol. 35, No. 13, 2006, pp.1631–51.

KELLY, J.M., Earthquake-resistant design with rubber. 2nd ed. ,1997, London: Springer.

KELLY, J.M., TSAI, H., "Seismic response of light internal equipment in base-isolated structures", Earthquake Engineering and Structural Dynamics, Vol. 13, No. 6, 1985, pp.711–32.

KONSTANTINIDIS, D., KELLY, J.M., MAKRIS, N., "Report No. UCB/EERC-2008/02: Experimental investigation on the seismic response of bridge bearings", Earthquake Engineering Research Center, University of California, Berkeley, 2008.

KONSTANTINIDIS, D., MAKRIS, N., "Experimental and analytical studies on the seismic response of freestanding and anchored laboratory equipment", Pacific Earthquake Engineering Research Center (PEER) University of California, Berkeley, Report No. 2005/07, 2005.

KONSTANTINIDIS, D., MAKRIS, N., "Experimental and analytical studies on the response of freestanding laboratory equipment to earthquake shaking", Earthquake Engineering and Structural Dynamics, Vol. 38, No. 6, 2009, pp.827–48.

KONSTANTINIDIS, D., MAKRIS, N., "Experimental and analytical studies on the response of 1/4-scale models of freestanding laboratory equipment subjected to strong earthquake shaking", Bulletin of Earthquake Engineering, Vol. 8, No. 6, pp.1457–1477.

KONSTANTINIDIS, D., NIKFAR, F., Seismic response of equipment and contents in base-isolated buildings subjected to broad-band ground motions. Earthquake Engineering & Structural Dynamic, Vol. 44, No. 6, 2015, pp.865–887.

MAKRIS, N., "Rigidity–plasticity–viscosity: can electrorheological dampers protect base-isolated structures from nearsource ground motions?", Earthquake Engineering and Structural Dynamics, Vol. 26, No. 5, 1997, pp.571–91.

MAKRIS, N., BLACK, C.J., "Dimensional analysis of rigid-plastic and elastoplastic structures under pulse-type excitations", Journal of Engineering Mechanics(ASCE), Vol. 130, No. 9, 2004, pp.1006–18.

MAVROEIDIS, G.P., PAPAGEORGIOU, A.S., "A mathematical representation of near-fault ground motions", Bulletin of the Seismological Society of America , Vol. 93, No. 3, 2003, pp.1099–131.

NEWMARK, N.M., "Effects of earthquakes on dams and embankments", Géotechnique, Vol. 15, 1965, pp.139–60.

NIKFAR, F., KONSTANTINIDIS, D., "Sliding response analysis of operational and functional components (OFC) in seismically isolated buildings", 3rd Specialty Conference on Disaster Prevention and Mitigation, Canadian Society of Civil Engineering (CSCE), Montreal, June 2013.

NIKFAR, F., KONSTANTINIDIS, D., "Solving dynamical systems with path-dependent nonlinearities using MATLAB ODE solvers", 10th National Conference in Earthquake Engineering, Earthquake Engineering Research Institute, Anchorage, AK, 2014.

SOMERVILLE, P., GRAVES, R., "Conditions that give rise to unusually large long period ground motions", The Structural Design of Tall Buildings , Vol. 2, No. 3, 1993, pp.211–32.

TAGHAVI, S., MIRANDA, E., "Response assessment of nonstructural building elements", Pacific Earthquake Engineering Research Center (PEER) University of California, Berkeley, Report No. 2003/05, 2003.

VASSILIOU, M. F., MAKRIS, N., "Analysis of the rocking response of rigid blocks standing free on a seismically isolated base", Earthquake Engineering and Structural Dynamics, Vol. 41, No. 2, 2012, pp.177–96.

VASSILIOU, M. F., MAKRIS, N., "Estimating time scales and length scales in pulse-like earthquake acceleration records with wavelet analysis", Bulletin of the Seismological Society of America, Vol. 101, No. 2, 2011, pp.596–618.

VELETSOS, A.S., NEWMARK, N.M., CHELEPATI, C.V., "Deformation spectra for elastic and elastoplastic systems subjected to ground shock and earthquake motions", Proceedings of the 3rd World Conference on Earthquake Engineering. Wellington, New Zealand, 1965.

XIA, F., Modelling of a two-dimensional Coulomb friction oscillator", Journal of Sound and Vibration, Vol. 265, No. 5, 2003, pp.1063-74.

YANG, T.Y., KONSTANTINIDIS, D., KELLY, J.M., “The influence of isolator hysteresis on equipment performance in seismic isolated buildings”, Earthquake Spectra, Vol. 26, No. 1, 2010, pp.275–293.